Indian J Phys (November 2015) 89(11):1183–1192
DOI 10.1007/s12648-015-0689-5

ORIGINAL PAPER

Effect of zinc substitution on molecular dynamics of protoporphyrin-IX

A Kumar and D Goswami*

Department of Chemistry, Indian Institute of Technology Kanpur, Kanpur 208016, India

Received: 10 November 2014 / Accepted: 24 March 2015 / Published online: 22 April 2015

Abstract: We report the effects of zinc metal substitution on the molecular dynamics of protoporphyrin-IX in dichloromethane solvent by spectrally resolving the femtosecond photon echo spectrum. We have found that the coherence and population dynamics change due to the presence of Zn metal in the protoporphyrin-IX system. Zinc metal reduces the conformational disorder in the molecular structure of protoporphyrin-IX and in turn increases the planarity of the molecule resulting in better delocalization of π-electrons in the system. This effect decreases the inhomogeneous broadening of the photon echo spectra of Zn-substituted protoporphyrin-IX.

Keywords: Photon echoes; Free induction decay (quantum optics); Femtosecond techniques in nonlinear optics

PACS Nos.: 78.47.jf; 42.50.Md; 42.65.Re

1. Introduction

The ultrafast nonlinear spectroscopic techniques are highly important in chemistry for understanding the structure and dynamics of complex molecular systems, such as porphyrins and laser dyes [1–3]. For these kinds of molecular systems, the spectroscopic techniques in time domain are useful because, in these systems, the quantum states are very congested and it becomes impossible to resolve the energy separation between them. This situation is more prevalent in the condensed phase, because in condensed phase, the environmental effects, such as solvent interaction and inter- or intra-molecular vibration, lead to the quasi-continuous states, which make the situation too complex to study their dynamics. The molecular dynamics of such systems can be studied by spectroscopic techniques, such as the hole burning, pump probe, up-conversion and photon echo techniques.

Out of these spectroscopic techniques, photon echo spectroscopy is the most powerful and reliable technique for the study of molecular dynamics [4–7]. This is because, by varying the time delay between the three ultrashort pulses, we can get two controlled time delays that would result in accurate information about the dynamics of the molecule. The time delay between the first two pulses is the coherence time (t_{12}), while the time delay between second and third pulses is called the population time (t_{23}). As a result of the interaction of three pulses in appropriate geometry and directions with the sample, a new electric field is generated in a specific direction that has information about the molecular dynamics of the sample [4–7]. These three pulses create a nonlinear polarization that comprises several molecular states with a definite phase relationship (coherence) amongst them. The coherence, which is strongly dependent on the electronic vibrational coupling mechanisms and the molecular environment can be used to manipulate and measure the third-order polarization generated by the interaction of multiple laser pulses. The measurement of nonlinear polarization in the time domain gives detailed information about the molecular dynamics. The application of multiple laser pulses with controllable time delays helps us to extract the complex dynamical and spectroscopic information, such as population relaxation times, dephasing times, inhomogeneous broadening and vibrational structure of transient species [8–14]. The main advantage of this technique is that the contribution of very slow or inhomogeneous broadening can be obtained [14]. Dao et al. [3] have applied the ultrafast photon echo spectroscopy to study the optical dephasing, ultrafast electron transfer and solvation dynamics in the dye molecule. The study of vibrational deactivation process in

*Corresponding author, E-mail: dgoswami@iitk.ac.in

picoseconds timescale has been done by two-colour three-pulse photon echo spectroscopy [15].

Earlier, we have used spectrally resolved photon echo (SRPE) technique to study the dynamics of metal-substituted octaethyle porphyrins [2]. All porphyrins are intensely coloured and represent an important class of molecules that are found in nature in different forms [16–20]. The metalloporphyrin ring is found in many important biological systems where it represents the active site. In fact, many metalloporphyrins play an important role in biological processes, such as the conversion of sunlight into chemical energy in plants using chlorophyll, oxygen transfer in blood using haemoglobin and myoglobin and also electron transfer in cytochrome-c and cytochrome oxidase [19]. Metalloporphyrin rings have potential in artificial solar energy harvesting system and molecular logic gates [20, 21]. The dependence of the SRPE spectra on varying metal centre in octaethyle porphyrin system has been reported earlier [2]. This has been done by varying the specific metal centre in octaethyle porphyrin and monitoring the molecular dynamics of the system. The dynamics changes are due to the unsymmetrical filling of electron in the metal orbital, which increases the asymmetry of the molecular structure [2]. The molecular dynamics of Zn-substituted cytochrome-c, Zn-tetraphenylporphyrin and Zn-protoporphyrin-IX has been reported for investigating the effects of protein conformation, axial ligation and solvent on the molecular dynamics by measuring the transition grating and photon echo signal [11].

In our present work, we have studied the molecular dynamics of protoporphyrin-IX and zinc-substituted protoporphyrin-IX to observe how the presence of zinc metal changes the coherence and population dynamics by SRPE spectroscopy.

2. Theoretical background

Spectrally resolved three-pulse photon echo peak shift techniques are mostly used for the study of molecular dynamics of complex molecular system, which are based on noncollinear four-wave mixing geometry under a specific phase-matching condition. In the particular experiments reported here, the incident laser beams propagate noncollinearly in box-car geometry as shown in Fig. 1. The three pulses in the box-car geometry are associated with the wave vectors: k_1, k_2 and k_3, which are focused onto the sample flow cell, so that after refocusing, the photon echo signal is generated at the fourth corner of the square. The first pulse k_1 creates coherence between the ground and the excited states and after that dephasing process start quickly. The second pulse k_2 interacts with the freely evolving system giving rise to a population grating in space, either in the ground state or in the excited state and no further dephasing occurs. The third pulse k_3 puts the system back into the second coherent state and after rephasing the signal is generated in $k_s = -k_1 + k_2 + k_3$. If the phase of the second coherent state is opposite to that of the first, then the contribution of photon echo signal is more in third-order nonlinear signal. However, if the phases of the first and second coherent states are same, then the contribution of the free induction decay (FID) type signal is more.

In this experiment, we have used the three ultrafast femtosecond pulses. These three ultrashort femtosecond pulses interact with system and induce the third-order nonlinear polarization ($P^{(3)}$) in sample as given by [13]:

$$P^{(3)} = \int_0^\infty \mathrm{d}t_3 \int_0^\infty \mathrm{d}t_2 \int_0^\infty \mathrm{d}t_1 E_1^*(t + t_{12} + t_{23} - t_3 - t_2 - t_1) \times E_2(t + t_{23} - t_3 - t_2) \times E_3(t - t_3) \times R^{(3)}(t_3, t_2, t_1) \quad (1)$$

where $R^{(3)}$ is a third-order nonlinear response function.

The third-order nonlinear response $R^{(3)}$ is a linear combination of both rephasing and nonrephasing response of the macroscopic dipole moment. It is given by:

$$R^{(3)}(t_1, t_2, t_3) = R_a(t_1, t_2, t_3) + R_b(t_1, t_2, t_3) \quad (2)$$

The rephasing (R_a) and nonrephasing (R_b) optical response function are given by:

$$R_a(t_3, t_2, t_1) = [R_2(t_3, t_2, t_1) + R_3(t_3, t_2, t_1)] \times E_3(t - t_{23} - t_3) \exp[-i\omega_3(t - t_{23} - t_3)] \times E_2(t - t_3 - t_2) \exp[-i\omega_2(t - t_3 - t_2)] \times E_1^*(t + t_{12} - t_3 - t_2 - t_1) \times \exp[i\omega_1(t + t_{12} - t_3 - t_2 - t_1)] \quad (3a)$$

$$R_b(t_3, t_2, t_1) = [R_1(t_3, t_2, t_1) + R_4(t_3, t_2, t_1)] \times E_3(t - t_{23} - t_3) \exp[-i\omega_3(t - t_{23} - t_3)] \times E_2(t - t_3 - t_2 - t_1) \exp[-i\omega_2(t - t_3 - t_2 + t_1)] \times E_1^*(t - t_{12} - t_3 - t_2) \exp[i\omega_1(t - t_{12} - t_3 - t_2)] \quad (3b)$$

where R_1 to R_4 and their complex conjugates are nonlinear response functions.

Nonlinear optical response theory is an important tool to understand the result and discussion part of our experiment. Figure 2(a) and 2(b) shows the Feynman diagrams representing the possible three-pulse interactions for the phase-matching direction [7]. We consider a two-electronic-state system with ground state S_0 comprising of two vibrational levels g and g' and an excited state S_1 with two vibrational levels e and e'. The first interaction is k_2, as shown in Fig. 2(a) and 2(b), that creates an optical coherence ($\rho = e'g$ or $\rho = eg$) and the pulsed ordering becomes 2–1–3, in which the phases of first coherent state is same as that of the second coherent state, resulting in a FID type signal. Also

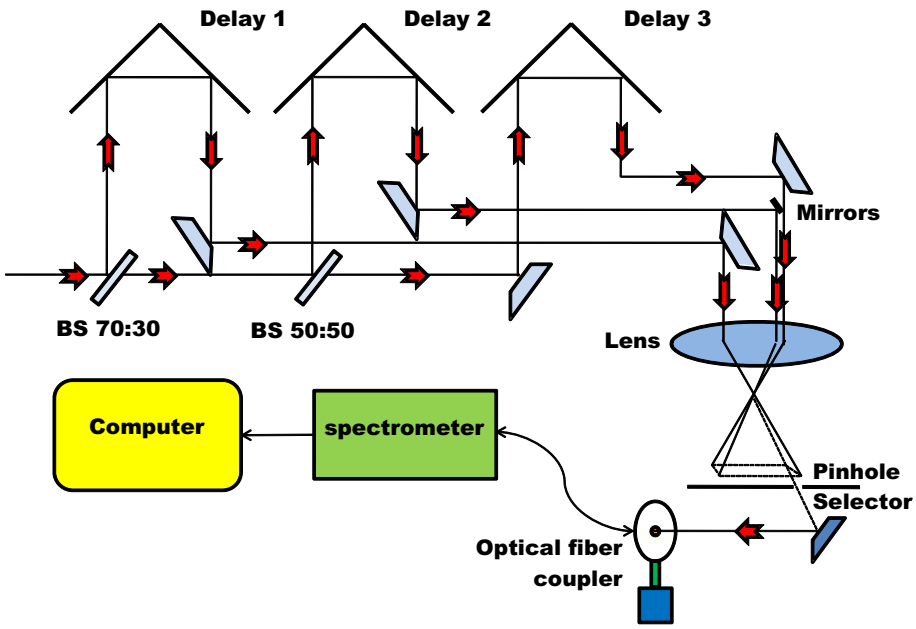

Fig. 1 Experimental details of our set-up: schematic of the three-pulse photon echo experimental set-up. Pulse sequence for three-pulse photon echo experiment

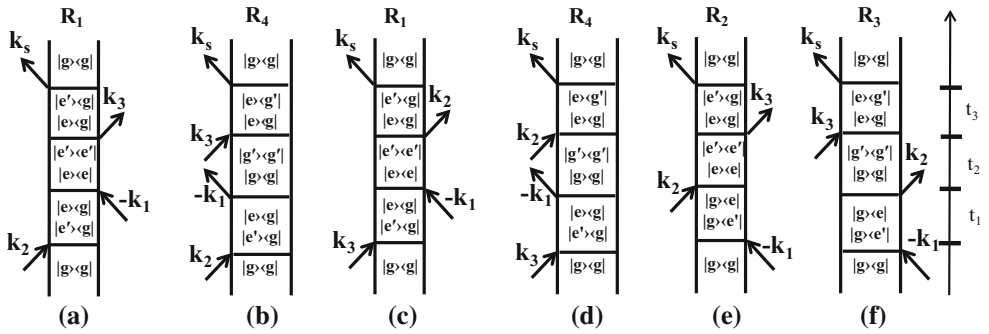

Fig. 2 Feynman diagrams to illustrate the interaction of three optical pulses associated with the wave vector k_1, k_2, and k_3 in the phase-matching direction $k_S = -k_1 + k_2 + k_3$ to result in the possible third-order nonlinear response signal as per their pulse interaction ordering: (**a**) pulse ordering 2–1–3 represents R_1 that follows the excited state pathway, (**b**) pulse ordering 2–1–3 represents R_4 that follows the ground state pathway, (**c**) pulse ordering 3–1–2 represents R_1 that follows the excited state pathway, (**d**) pulse ordering 3–1–2 represents R_4 that follows the ground state pathway, (**e**) pulse ordering 1–2–3 represents R_2 that follows the excited state pathway, and (**f**) pulse ordering 1–2–3 represents R_3 that follows the ground state pathway

when the first interaction is k_3, as shown in Fig. 2(c) and 2(d), the third pulse creates a contribution to the optical coherences ($\rho = e'g$ or eg and $\rho = eg'$ or eg), in which the phases of first coherent state are same as that of second coherent state, resulting in a FID signal. Therefore, nonlinear response functions R_1 and R_4 contribute as the FID signal. When the time ordering of the pulses is k_1, k_2, k_3, as shown in Fig. 2(e) and 2(f), and the three laser pulses are tuned from g to e or e', the first pulse k_1 creates optical coherences ($\rho = ge'$ or $\rho = ge$) and the second pulse k_2 generates population in either excited state ($\rho = e'e'$ or $\rho = ee$), as shown in Fig. 2(e). The third pulse k_3 converts the populations back into optical coherences ($\rho = e'g$ or $\rho = eg$), in which the phases of the frequency components are opposite to those of the initial optical coherence contributions. Thus, photon echo signal is produced by the rephasing of the macroscopic polarization at time period $t = t_{12}$ after the third pulse in the phase-matching direction $k_s = -k_1 + k_2 + k_3$ for an inhomogeneously broadened ensemble. The relevant nonlinear response function for this pathway is R_2, as shown in Fig. 2(e). However, if the ground state pathway is followed as in Fig. 2(f), the relevant response function would be R_3. Thus, the response functions R_1 and R_2 follow the excited state pathway, while R_3 and R_4 response functions follow ground state pathway.

Now, the Gaussian distribution for a simple two-level system with inhomogeneous broadening is given by

$$G(\omega) = \exp\left[-\frac{(\omega-\omega_{12})^2}{2}\right] \tag{4}$$

where Γ is 1/e half-width. The nonlinear response function is given by

$$\begin{aligned} R_1(t_3,t_2,t_1) &= \exp[-i\omega_{12}(t_3+t_1)]\exp[-\gamma_{12}(t_3+t_1)] \\ &\quad\times\exp[-\gamma_{12}t_2]\exp\left[-\Gamma^2(t_3+t_1)^2\Big/4\right] \\ &= R_4(t_3,t_2,t_1) \end{aligned} \tag{5a}$$

$$\begin{aligned} R_2(t_3,t_2,t_1) &= \exp[-i\omega_{12}(t_3-t_1)]\exp[-\gamma_{12}(t_3+t_1)] \\ &\quad\times\exp[-\gamma_{12}t_2]\exp\left[-\Gamma^2(t_3-t_1)^2\Big/4\right] \\ &= R_3(t_3,t_2,t_1) \end{aligned} \tag{5b}$$

where ω_{12} is the transition frequency, $\gamma_{12} = 1/T_2$ and $\gamma_1 = 1/T_1$. The T_1 is the life time of excited state and T_2 is the dephasing time of the transition. Finally, the spectrally resolved third-order nonlinear signal recorded in the spectrometer is given by

$$S(\lambda_d,t_{12},t_{23}) \propto \int_0^\infty \left|P^{(3)}(\lambda_d,t_{12},t_{23})\right|^2 \mathrm{d}t \tag{6}$$

where λ_d is the wavelength detected by the spectrometer.

3. Experimental details

Protoporphyrin-IX and Zn-protoporphyrin-IX (Sigma Aldrich) were dissolved in di-chloromethane (DCM) solvent to produce 10^{-4} molar concentration solutions. The schematic of our experimental set-up, as shown in Fig. 3, comprised. The set-up comprised of a laser system having the Ti:sapphire oscillator pulses with pulse width of 20 fs at 800 nm. This 94-MHz train of pulses seeded a commercial Ti:sapphire multipass amplifier (ODIN, Quantronix Corp.), which was pumped by a Nd:YAG laser operating at 1 kHz (Corona, Coherent Inc.). The amplified laser generated 1-kHz pulses with a pulse width of 40 fs at a central wavelength of 806 nm. These amplified pulses were used to pump a commercial computer-controlled travelling wave optical parametric amplifier (TOPAS, Light Conversion Ltd.). In the optical parametric amplifier (OPA), a small fraction of the pump from the multipass amplifier was used to generate the parametric super fluorescence seed in a thick beta barium borate (BBO) crystal. These pulses from the OPA were tuneable across the visible region of the spectrum with ~50-fs pulse width. The output of the OPA was divided into three beams of nearly equal intensity and focused in box-car geometry, as shown in Fig. 3 into a flow cell having a path length of 0.2 mm. The third-order nonlinear signal appeared at the fourth corner of the square, which was collected through an optical fibre coupled with Ocean optics Spectrometer (HR-2000).

4. Results and discussion

The central wavelength of the laser pulses is tuned to 530 nm, which is near the Q-band of the porphyrin system where a weak transition occurs between S_0 and S_1. The S_0 to S_2 transition in porphyrin system occurs at 400 nm. This is called the Soret band or the B-band. The internal conversion from S_2 to S_1 is so rapid that the fluorescence is detected from the S_1 state. Both the B-band and Q-band arise from π to π^* transitions and can be explained by Gouterman's four-orbital model [17]. In porphyrin systems, two bands are observed in the visible region between 500 and 600 nm. These two bands are separated by 1250 cm^{-1}. The Q_{00} is the lowest energy band, which is the electronic origin for the lowest excited state energy. The second Q_{01} band is the higher energy band that includes one additional mode of vibrational excitation [17].

In our particular experiments, we are using protoporphyrin-IX and Zn-protoporphyrin-IX to study their molecular dynamics. The point group for these molecules, when they are in their planar structure, is C_s. However, the absorption bands for Zn-protoporphyrin-IX arise from the linear combination of the nearly degenerate electronic states

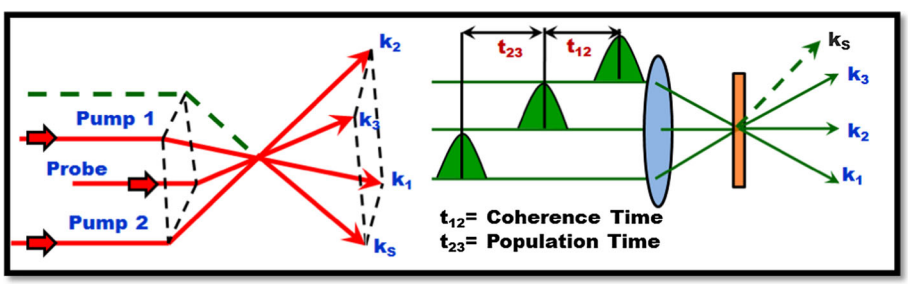

Fig. 3 Pulse sequence for the three-pulse photon echo experiment

within the quasi D_{4h} molecular symmetry under the Gouterman's four-orbital model [22]. The two electronic transitions terminate in the lowest empty orbital, which is e_g for Zn-protoporphyrin-IX. Both e_{gx} and e_{gy} are possible as they are degenerate and are of e_g symmetry. The Q_{00} band transition originates in the highest filled orbital (HOMO), which is of a_{2u} symmetry. The B-band transition originates in the next highest filled orbital, which has a_{1u} symmetry. Electronic states resulting from optical transitions between the orbitals a_{1u} to e_{gx} and a_{2u} to e_{gy} are of first order. The configuration interaction between states having the same polarizations get mixed, which then splits the states into two pairs of high-energy (B_x and B_y) and low-energy (Q_{00} and Q_{10}) transitions. For investigating the ground and excited states, this D_{4h} point group for the zinc-substituted protoporphyrin-IX reduces to D_{2h} point group for protoporphyrin-IX by the replacement of zinc metal with two protons in the porphyrin rings [23, 24]. The molecular orbitals for the protoporphyrin-IX molecule are: a_u, b_{1u}, b_{2u} and b_{3g} respectively, where the x and the y molecular axes are not equivalent. The x molecular axis is defined through the central nitrogen electron lone pairs, while the y molecular axis is defined through the central N–H bonds. Thus, the excited states resulting from transitions between the orbitals are not degenerate and the spectroscopic transitions are expected to be split into distinct bands [25]. For metalloporphyrins, the Q-band splits into Q_{00} and Q_{10} bands, when embedded in a Shpolskii matrix [26, 27]. The crystal field causes a splitting of the Q-band and reduces the D_{4h} symmetry of the metalloporphyrin [28, 29]. This splitting has a close relationship to the local field in the molecule. So the investigation of Q-band splitting gives information about the porphyrin local field. The investigation of Q_{00} and Q_{10} bands also plays an important role in understanding the nearly degenerate structure of the metalloporphyrin absorption spectrum, which sometimes shows a significant barrier to site-selective spectroscopy [30, 31].

The contour plots of SRPE signal of protoporphyrin-IX are given in Fig. 4(a)–4(d), where we have varied the coherence time (t_{12}) at different fixed population times (t_{23}) as 0, 50, 100 and 200 fs, respectively. At zero delay (i.e. population time, $t_{23} = 0$ fs), the signal intensity is maximum near zero coherence time (t_{12}) as show in Fig. 4(a). For negative coherence times ($t_{12} < 0$ fs), the contribution of FID signal is more in the photon echo spectra according to the Feynman diagram, as shown in Fig. 2(a) and 2(b). This is because, at negative coherence times, the second pulse interacts with the system first and the pulse ordering in the system becomes: 2–1–3. With this pulse ordering, the nonrephasing response function (R_1 or R_4) contributes more to the spectra as the phase of two coherent states are the same, as given by Eq. (5a). For positive coherence time ($t_{12} > 0$ fs), the contribution of photon echo-like signal is more because, in this case, the first pulse interacts with the system first resulting in a pulse ordering of 1–2–3 in the Feynman diagram. With this pulse ordering, the rephasing response function (R_2 or R_3) contributes to the spectra, as given by Eq. (5b). The tilted profile in Fig. 4(a)–4(d) show that the spectra is blue-shifted for negative coherence time and red-shifted for positive coherence time, indicating the presence of inhomogeneous broadening in the spectrum until $t_{23} \geq 200$ fs. At 200-fs population time, the signal intensity has almost decayed, as shown in Fig. 4(d), due to the weak population grating formed by the first two pulses. This persistence of inhomogeneous spectral broadening to a long timescale can be attributed to the lesser symmetry in the molecular structure of protoporphyrin-IX (D_{2h} point group in comparison with D_{4h} for the other porphyrin systems [22, 28]. As we increase the population times, the signal intensity decreases because the system has no memory to rephase or dephase at longer population times. Figure 4(a)–4(d) show that the peak of SRPE signal is red-shifted from 530 to 538 nm as the fixed population time changes from 0 to 200 fs. This indicates the coherence time-dependent spectral broadening of photon echo signal and the population relaxation dynamics for protoporphyrin-IX.

Figures 5(a) and 4(d) represent the three-dimensional (3D) plots of SRPE signals by varying the coherence time at respective fixed population times of 0, 50, 100 and 200 fs. We find from Fig. 5(a)–5(d) that there is a continuous increase in the intensity of the third-order nonlinear signal as the coherence time goes to the zero delay from either positive or negative directions. There is a clear red-shift on increasing the fixed population time (t_{23}), while the coherence time (t_{12}) varies systematically, which indicates coherence time-dependent spectral broadening and population relaxation dynamics.

Figures 6(a)–6(d) and 7(a)–7(d) show the contour and 3D plots of SRPE signal of Zn-protoporphyrin-IX by varying the coherence time at specific fixed population times (t_{23}) of 0, 50, 100 and 200 fs, respectively. The tilted profile of photon echo spectra shown in Fig. 6(a) has blue-shift towards the negative coherence time and red-shift towards the positive coherence time, indicating inhomogeneous broadening in the spectra. The signal intensity is maximum towards the negative coherence time. In Fig. 6(b), the spectrum starts becoming symmetrical with respect to the zero coherence time and the signal intensity maxima is shifted towards the zero coherence time. In Fig. 6(c) at 100-fs population time, the spectrum is maximized at zero coherence time and is almost symmetrical with respect to the zero coherence time. Thereafter, no further wavelength shift is observed as we increase the fixed population time from 50- to 100-fs timescale as shown in Fig. 6(b) and 6(c). This indicates that the inhomogeneous broadening in the spectrum is no longer present

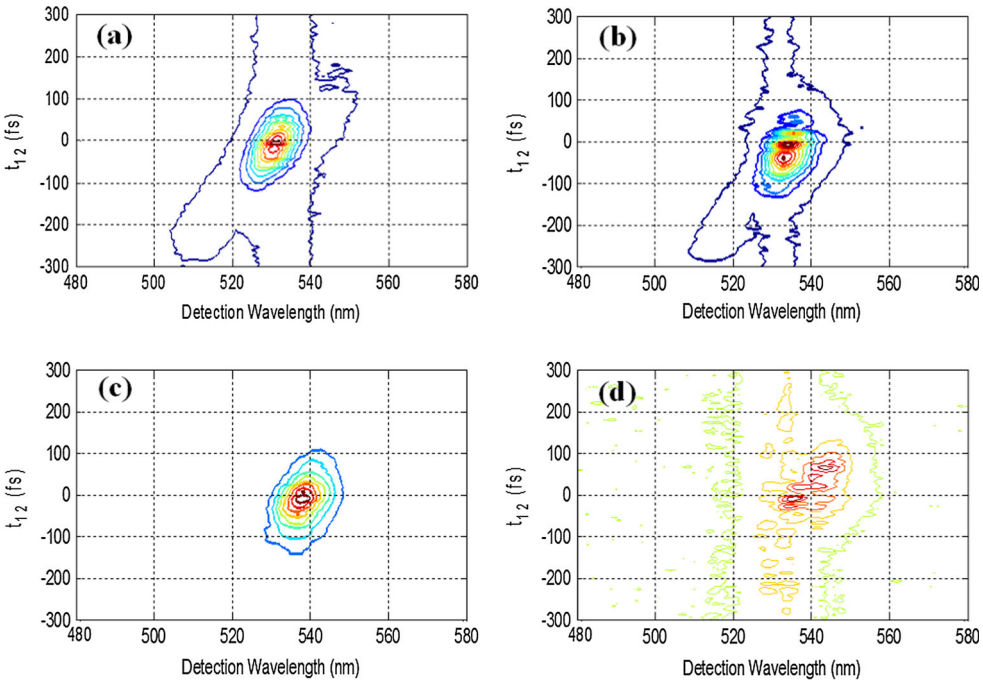

Fig. 4 Contour plots of the third-order nonlinear signal (coherence time t_{12}) for protoporphyrin-IX in DCM solvent at different population times (t_{23}): (**a**) $t_{23} = 0$ fs, (**b**) $t_{23} = 50$ fs, (**c**) $t_{23} = 100$ fs, and (**d**) $t_{23} = 200$ fs

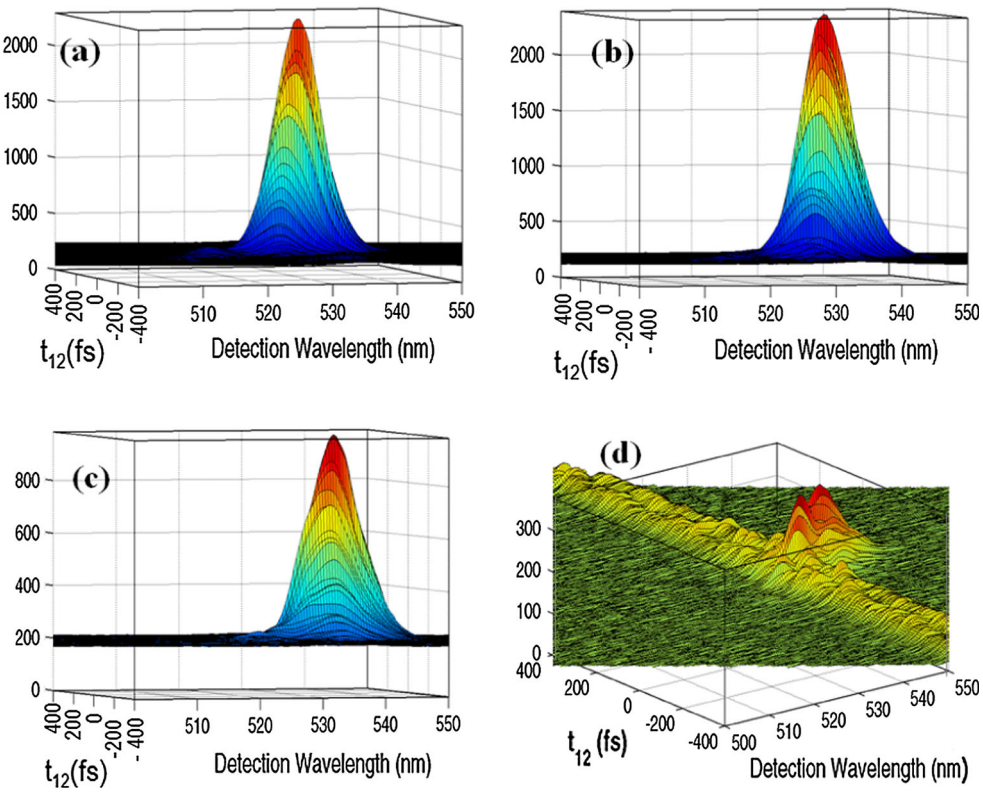

Fig. 5 Three-dimensional plots of the third-order nonlinear signal (coherence time t_{12}) for protoporphyrin-IX in DCM solvent at different population times (t_{23}): (**a**) $t_{23} = 0$ fs, (**b**) $t_{23} = 50$ fs, (**c**) $t_{23} = 100$ fs, and (**d**) $t_{23} = 200$ fs

beyond 50-fs time delay. Furthermore, this indicates the spectral diffusion process occurs within 100-fs timescale for zinc-substituted protoporphyrin-IX. The spectral diffusion process at such short timescales may occur due to zinc substitution, which increases the symmetry of the protoporphyrin-IX molecule from D_{2h} point group to D_{4h} point group. This increase in symmetry decreases the conformation disorder of the molecule and leads to a lesser inhomogeneous broadening as compared to protoporphyrin-IX.

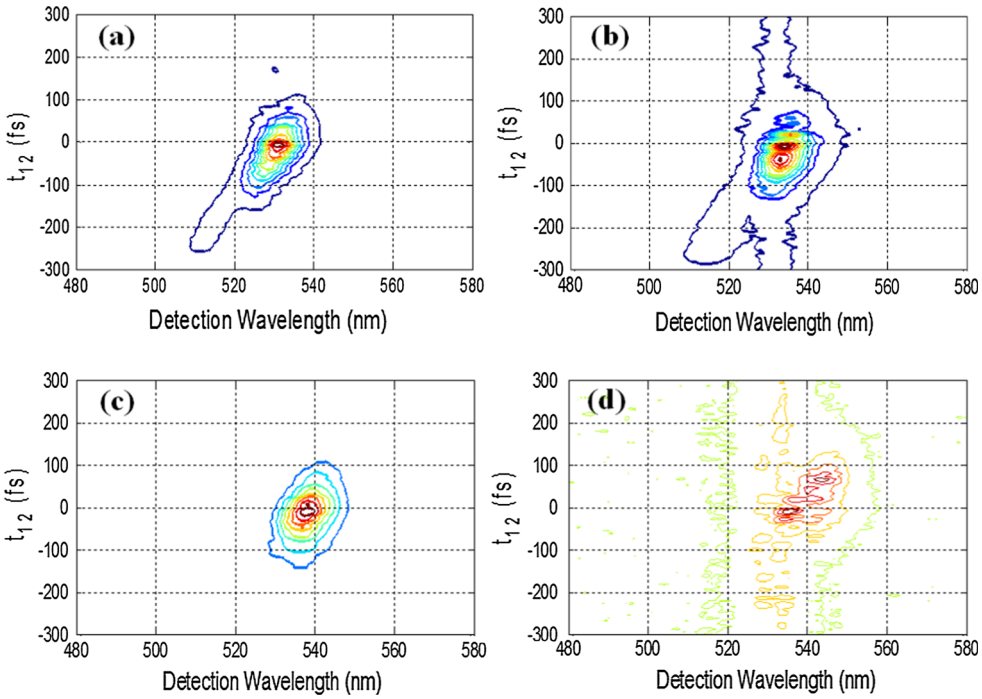

Fig. 6 Contour plots of the third-order nonlinear signal (coherence time t_{12}) for Zn-protoporphyrin-IX in DCM solvent at different population times (t_{12}): (**a**) $t_{23} = 0$ fs, (**b**) $t_{23} = 50$ fs, (**c**) $t_{23} = 100$ fs and (**d**) $t_{23} = 200$ fs

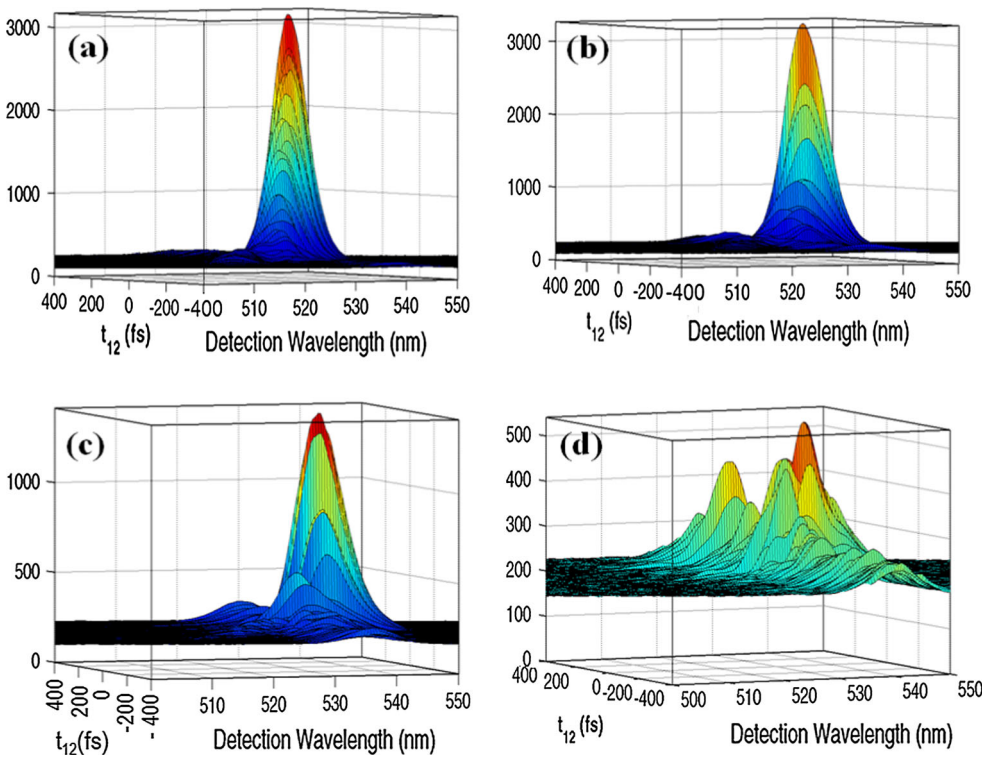

Fig. 7 Three-dimensional plots of the third-order nonlinear signal (coherence time t_{12}) for Zn-protoporphyrin-IX in DCM solvent at different population times (t_{23}): (**a**) $t_{23} = 0$ fs, (**b**) $t_{23} = 50$ fs, (**c**) $t_{23} = 100$ fs and (**d**) $t_{23} = 200$ fs

From Fig. 7(a)–7(d), we find that there is a continuous increase in the intensity of the third-order nonlinear signal as the population time approaches zero delay from either positive or negative directions. Also there is a continuous red-shift on increasing the fixed population time (t_{23}) from 0 to 50 fs, indicating population relaxation dynamics. The signal intensity continuously decreases as we increase the fixed coherence time from 0 to 200 fs. Actually, the signal is due to the scattering of the third pulse on the grating formed by the overlapping tails of the FIDs of the first two

pulses. Thus, the increase in delay between the first two pulses decreases the intensity of the measured signal as shown in Fig. 7(a)–7(d).

Time-resolved optical spectroscopy or time-resolved photon echo spectroscopy gives valuable information about the population relaxation timescales. For the population relaxation timescales, laser pulses are tuned to the long wavelength tail of Q_{01} band of the protoporphyrin-IX system. We have used the pulse sequence of three laser pulses as shown in Fig. 3. The measurement of time-dependent photon echo signal as a function of population time (t_{23}) at different fixed coherence time (t_{12}) gives information about the electronic and vibrational relaxation time periods. The short timescale (τ_1) recovered from our experimental measurements given in Table 1 is sub-50 fs as it is limited by our instrument resolution of sub-50-fs pulses. The population decay of protoporphyrin-IX is in order of 6 ps or larger [32], which our femtosecond-pulsed experiments are unable to measure and the time-integrated plots in Fig. 8 are simply single-exponential decays limited by our laser pulse width. However, we find that the population decay timescales for the Zn-protoporphyrin-IX is much faster, as shown in Fig. 9(a)–9(d) and their time-integrated plots show a bi-exponential decay. Thus, for the Zn-protoporphyrin-IX at zero delay or at zero coherence time (t_{12}), i.e. when the first and the second pulses arrive simultaneously, the two decay terms are: 42 and 321 fs respectively, as shown in Table 1. The fitted bi-exponential curves at fixed coherence time (t_{12}): 0, 50, 100, and 200 fs, are shown in Fig. 9 and the corresponding measured decay timescales are shown in Table 1. As in case of protoporphyrin-IX, we note that the fast decay components (τ_1) of the integrated plots for Zn-protoporphyrin-IX are also pulse width-limited (sub-50 fs). The τ_2 component of Zn-protoporphyrin-IX is being reported here for the first time.

Thus, in case of Zn-protoporphyrin-IX, the π–π electronic interaction is more as a result of the better planarity of the molecule. The zinc metal substitution increases the symmetry of the protoporphyrin-IX, which can be the reason for the much faster timescales for Zn-protoporphyrin-IX as compared to that of protoporphyrin-IX. In our experiments, from the above observed decay timescales, it can be concluded that the ultrafast relaxation of the population placed in Q_{10} occurs in less than 50 fs. This fast

Table 1 Population relaxation timescales of Zn-protoporphyrin-IX

Coherence time (t_{12}; fs)	Decay constant (τ_1; fs)	Decay constant (τ_2; fs)
$t_{12} = 0$	43	321
$t_{12} = 50$	44	392
$t_{12} = 100$	47	440
$t_{12} = 200$	46	465

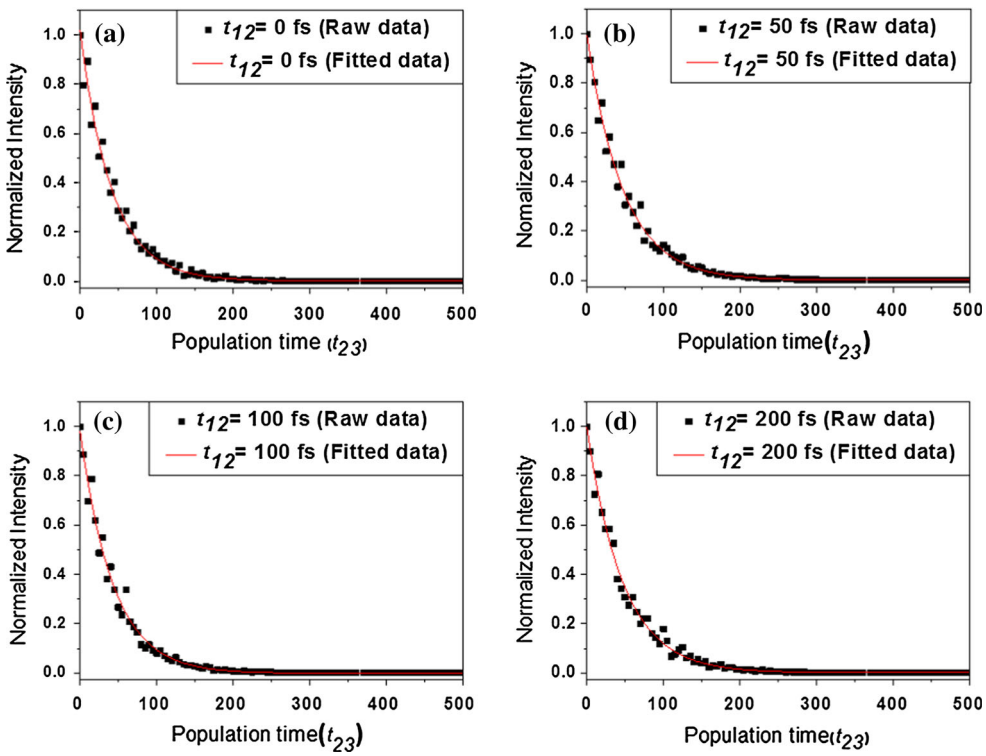

Fig. 8 Fitted integrated plots of (population time t_{23}) photon echo signal for protoporphyrin-IX in DCM solvent for different coherence times (t_{12}): (**a**) $t_{12} = 0$ fs, (**b**) $t_{12} = 50$ fs, (**c**) $t_{12} = 100$ fs and (**d**) $t_{12} = 200$ fs. All the plots are single-exponential fits limited by the pulse width of the laser used in the experiment

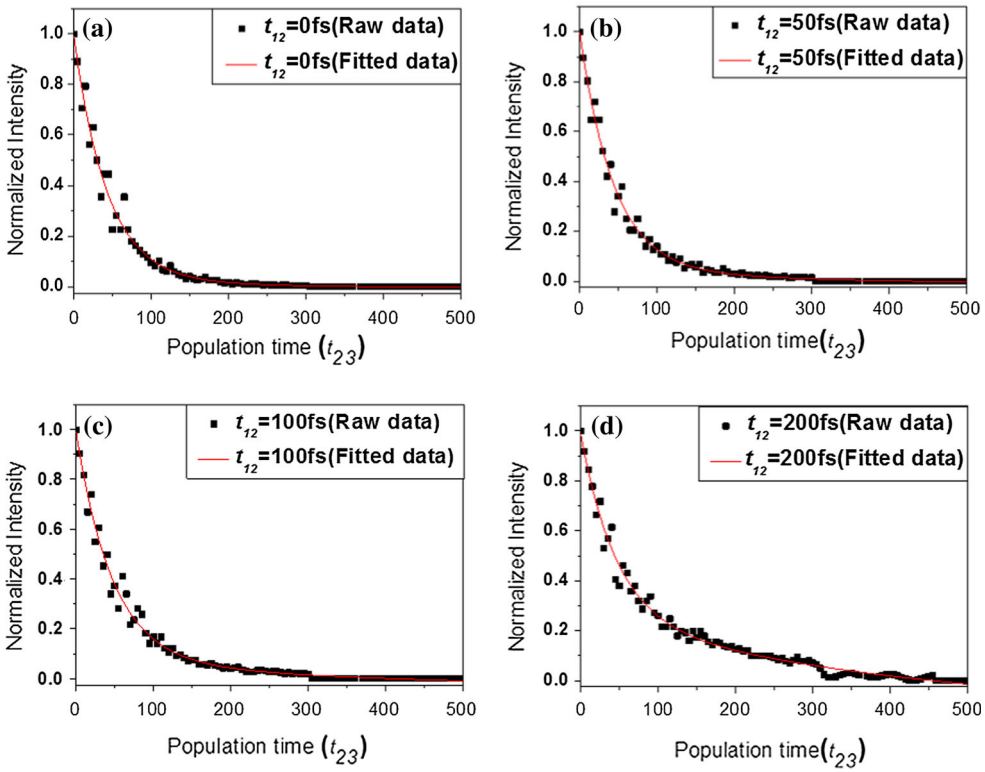

Fig. 9 Fitted integrated plots of (population time t_{23}) photon echo signal for Zn-protoporphyrin-IX in DCM solvent for different coherence times (t_{12}): (**a**) $t_{12} = 0$ fs, (**b**) $t_{12} = 50$ fs, (**c**) $t_{12} = 100$ fs and (**d**) $t_{12} = 200$ fs

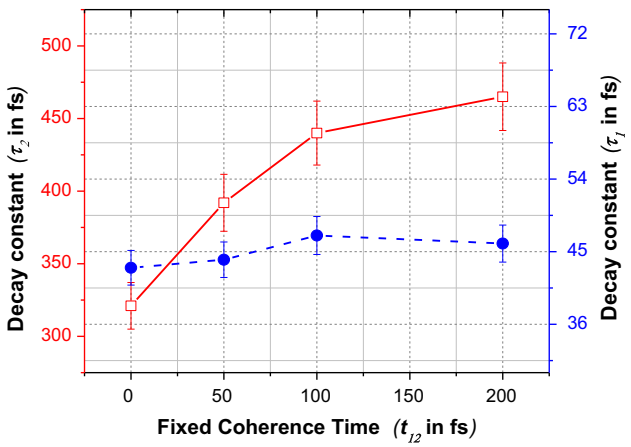

Fig. 10 Relative change of the decay times (τ_1 and τ_2) at specific coherence times (t_{12}) with experimental error bars for Zn-protoporphyrin-IX in DCM solvent

decay timescale is related to the electronic relaxation of Q_{01} to Q_{00}. The intra-molecular vibrational redistribution of Q_{00} state may be related to the longer relaxation timescales. Finally, we focus on the relative change of the decay times (τ_1 and τ_2) at specific coherence times (t_{12}) for Zn-protoporphyrin-IX, as shown in Fig. 10(a)–10(d). We find that while the faster decay times (τ_1) and the experimental laser pulse width are constant within the experimentally measurable errors, there is a consistent increase in the longer decay time (τ_2).

5. Conclusions

The spectral diffusion process occurs at ~100-fs timescale for Zn-protoporphyrin-IX. For protoporphyrin-IX, the tilted profile is still present at 200-fs timescale though the signal almost has decayed by that time. This shows that the inhomogeneous broadening in the SRPE plots persisted from 0- to 200-fs population time (t_{23}). Equivalently, we can say that the spectral diffusion process may occur after 200-fs timescale. In our previously published paper on octaethyle porphyrin, the signal is not enough to be detected. It may be due to symmetrical structure of octaethyle porphyrin by the presence of four ethyl group at the outer part of the porphyrin molecule. But in case of protoporphyrin, the molecular structure is not very much symmetric. This dissymmetry comes from the absence of D_{4h} point group because of the unsymmetrical substituted functional group on the outer part of the porphyrin molecule. The inhomogeneous broadening in the photon echo spectrum is more in case of protoporphyrin-IX as compared to Zn-protoporphyrin-IX. This is because the molecular structure of Zn-protoporphyrin-IX is more symmetric as compared to protoporphyrin-IX due to the presence of zinc metal ion. Zinc metal increases the planarity of the molecular structure of the porphyrin system that helps in delocalization of π-electrons and also creates more π–π interaction in the system, thereby affecting the molecular dynamics of the system. Peak shift is directly proportional to the

inhomogeneous broadening in the spectrum. Thus the higher red-shift in the photon echo spectrum for protoporphyrin-IX as compared to that of zinc-substituted protoporphyrin-IX is due to the presence of its inhomogeneous broadening at longer timescales. Time-integrated photon echo signals for protoporphyrin-IX and Zn-substituted protoporphyrin-IX show two different timescales. The electronic relaxation timescale for Q_{10} state is found to be within sub-50 fs for both protoporphyrin-IX and Zn metal-substituted protoporphyrin-IX, which is laser pulse width-limited. For zinc metal-substituted protoporphyrin-IX, the intramolecular vibrational relaxation occurring in Q_{00} band is found to be in between 321 and 465 fs at different fixed coherence time.

Acknowledgments D.G. thanks the support from the Department of Science and Technology (DST) Swarnajayanti Fellowship, Indian Space Research Organization (ISRO) Space Technology Cell funds, and Ministry of Human Resource Development (Govt. of India) for funding this research. A.K. acknowledges Council of Scientific and Industrial Research (CSIR), India, for graduate fellowship.

References

[1] B M Cho, C F Carlsson and R Jimenez *J. Chem. Phys.* **124** 144905 (2006)
[2] S K K Kumar, V Tiwari, T Goswami and D Goswami *Chem. Phys. Lett.* **476** 31 (2009)
[3] L V Dao, C Lincoln, M Lowe and P Hannaford *J. Chem. Phys*. **120** 8434 (2004)
[4] S Mukamel *Principles of Nonlinear Optical Spectroscopy* (eds.) M Lapp, J-I Nishizawa, B B Snavely, H Stark, A C Tam and T Wilson (New York: Oxford University Press) Ch 6, p 299 (1995)
[5] W P de Boeij, M S Pshenichnikov and D A Wiersma *Chem. Phys.* **233** 287 (1998)
[6] Y R Shen *The Principles of Nonlinear Optics* (eds) A Brignon and J-P Huignard (New York: Wiley-Interscience) Ch 14, p 242 (1984)
[7] P Hannaford *Femtosecond Laser spectroscopy* (Boston: Springer) Ch 8, p 197 (2005)
[8] J D Hybl, A A Ferro and D. M. Jonas *J. Chem. Phys.* **115** 6606 (2001)
[9] S M G Faeder and D M Jonas *J. Phys. Chem. A* **103** 10489 (1999)
[10] J D Hybl, A W Albrecht, S M G Feader and D. M. Jonas *Chem. Phys. Lett.* **297** 307 (1998)
[11] A W Albrecht, J D Hybl, S M Sarah, S M G Feader and D M Jonas *J. Chem. Phys.* **111** 10934 (1999)
[12] S Mukamel, A Piryatinski and V Chernyak *Acc. Chem. Res.* **32** 145 (1999)
[13] A Tokmakoff, A S Kwok, R S Urdahl, R S Francis and M D Fayer *Chem. Phys. Lett.* **234** 289 (1995)
[14] T Joo, Y Jia, J Yu, M J Lang and G R Fleming *J. Chem. Phys*. **104** 6089 (1996)
[15] W Zinth and W Kaiser *Topics in Applied Physics* (Heidelberg: Springer-Verlag) Vol. 60 p 235 (1998)
[16] K M Smith *Porphyrins and Metalloporphyrins* (Amsterdam: Elsevier) Ch 1 p 6 (1975)
[17] M Boulton, M Różanowska and B Różanowski *J. Photochem. Photobiol. B: Biol.* **64** 144 (2001)
[18] E I Sagun, E I Zenkevich, V N Knyukshto, A M Shulga, D A Starukhin and C V Borczyskowski *Chem. Phys.* **275** 211 (2002)
[19] L R Milgrom *The Color of Life* (New York: Oxford University Press) Ch 4 p 112 (1997)
[20] X Liu, E K L Yeow, S Velate and R P Steer *Phys. Chem. Chem. Phys*. **8** 1298 (2006)
[21] P Heathcote, P K Fyfe and M R Jones *Biochem Sci.* **27** 79 (2002)
[22] A Ceulemans, W Oldenhof, C Gorller-Warland and L G Vanquickenborne *J. Am. Chem. Soc.* **108** 1155 (1986)
[23] M Filatov, N Harris and S Shaik *J. Chem. Soc. Perkin Trans.* **2** 399 (1999)
[24] T G Spiro and T C Strekas *Proc. Nat. Acad. Sci.* **69** 2622 (1972)
[25] C Bruckner et al. *Chem. Phys.* **294** 285 (2003)
[26] G W Canters, J van Egmond, T J Schaafsma and J H van der Waals *Mol. Phys.* **24** 1203 (1972)
[27] J Bohandy and B F Kim *Spectrochim. Acta Part A* **35** 415 (1979)
[28] D Dolphin *The Porphyrin* (New York: Academic) Vol. 3 Ch 1, p 11 (1978)
[29] G W Canters *J. Chem. Phys.* **74** 157 (1981)
[30] J S Ahn, Y Kanematsu, Y Nishikawa and T Kushida *Synth. Met.* **71** 1735 (1995)
[31] Y Shibata, A Kurita and T Kushida *J. Lumin.* **66–67** 13 (1996)
[32] A Marcelli, I J Badovinac, N Orlic, P R Salvic and C Gellini *Photochem. Photobiol. Sci.* **12** 348 (2013)